DRAFT VERSION FEBRUARY 7, 2020
Typeset using LaTeX **twocolumn** style in AASTeX62

Extreme outflow of Enormous Lyα Nebula in MAMMOTH-1

Shiwu Zhang[1] and Zheng Cai[1]

[1]*Department of Astronomy, Tsinghua University, Shuangqing Road No.30, Haidian Beijing China*

Abstract

1. Introduction

It has been realized over the past decade that the black hole(BH) at the centre of a galaxy bulge is no mere ornament but may play a major role in galaxy evolution. The process by which this occurs is known as AGN(Active Galactic Nucleus) feedback and it takes place through an interaction between the energy and radiation generated by accretion onto the massive BH and the gas in the host galaxy. In contrast to the large ratio of the size of BH to host galaxy, AGN have a potent effect on galaxy formation and evolution even the large-scale structure. For example, the energy released to build a BH with mass $M_{BH} = 10^8 \mathbf{M}_\odot$ would correspond to $E_{BH} \approx 0.1 M_{BH} c^2$. This total accretion energy is two-to-three order of magnitude higher than the binding energy of the galaxy bulge in which this BH is reside, and is comparable to, even higher than, the thermal energy of the gas in the dark matter halo in which this galaxy resides(Harrison (2016)). So the study on AGN feedback is extremely important for galaxy even cosmology.

Theoretical models of galaxy formation and evolution have found it necessary to implement AGN feedback processes in order to produce the observational evidence. There are two sorts of AGN feedback divided according to mechanism. The first one is radio mode feedback also known as maintenance mode or kinetic mode, this mode is thought to be most efficient in the most massive halos, at late times and during periods of low BH accretion rates. The objects that are responsible for this type of feedback are likely to be low-excitation radio AGN which has low accretion rate and is always companied by radio lobes(Churazov et al. (2005);Bower et al. (2006);McCarthy et al. (2011)). This method of feedback is mainly use to explain the cut-off at the bright of the galaxy luminosity function in cluster environment(Bower et al. (2006);Croton et al. (2006);Somerville et al. (2008)). In contrast, a more catastrophic form of interaction between AGN and their host galaxies is proposed during periods of rapid accretion known as quasar mode or radiative mode. The objects are predicted to be responsible for this type of feedback are the radiatively-efficient AGN which has large accretion rate. Theoretical models that invoke this form of feedback typically require $\approx 0.005 - 0.15$ of the accretion energy to couple to the cold gas within the host galaxy and to expel this gas through outflows which ultimately results in the shut-down of future BH growth or star formation(Benson et al. (2003);Hopkins & Beacom (2006);DeBuhr et al. (2012)). In addition, analytical models have used the idea of galaxy-scale outflows initially launched by AGN, to explain $M_{BH} - M_{bulge}$ relationship(Fabian (1999);Granato et al. (2004);King et al. (2011);Faucher-Giguère & Quataert (2012)). While this form of feedback has been predicted to be effective at producing high mass outflow rates and quench star formation. In addition to the potential affects of AGN feedback described above, AGN-driven outflows may be required to blow the gas in their host galaxy out to explain the chemical enrichment of intercluster medium(ICM) and circumgalactic medium(CGM)(Borgani et al. (2008);Wiersma et al. (2009);Fabjan et al. (2010);Ciotti et al. (2010)). It has also been prompted that, in some cases, these outflows could induce positive feedback which trigger star formation by inducing pressure in cold gas reservoirs(Nayakshin & Zubovas (2012);Ishibashi & Fabian (2012);Silk (2013)). So the theory of galaxy formation and evolution strongly depends on AGN feedback models. However, there are still many problems to be solved, it is not well established how the accretion energy couples to the gas to drive outflows and the impact of outflow on a much larger physical scale. Observations are required to constrain the details of how, when and where these processes actually occur.

It is believed that AGN activity is required to drive the highest velocity outflows and are particularly important for the evolution of most massive galaxies(Benson et al. (2003);McCarthy et al. (2011);Harrison et al. (2018)). AGN-driven outflows are initially launched from the accretion disk or dusty torus surrounding the BH. Usually, spatially resolved spectroscopy is used as a direct way to search for and characterize outflows. Such observations have identified outflows in ionized, atomic and molecular gas(Nesvadba et al. (2008)). A diagnostic that is commonly used to search for outflowing ionized gas is broad, asymmetric and high-velocity OIIIλ5007 emission line. This is the good tracer of kinematics in the narrow-line region(NLR) of AGN and people have used it to study kinematics in hundreds to ten of thousands of AGN(Wang et al. (2011);Mullaney et al. (2013)) to constrain the ubiquity of these outflow features and study them as a function of key AGN properties.

These studies have used only one-dimensional spectra and therefore provide no insight on the spatial extent or structure of the outflows. Even for long-slit spectroscopy one only ob-

zsw18@mails.tsinghua.edu.cn

tain a spectrum of the light that actually passes through the slit(all other light is lost). However, the spatial information is crucial to study the outflow, such as the sphere of influence, kinematic energy and momentum. These information help to understand how feedback influence evolution of host galaxy, furthermore, how it change the large-scale kinematics environment. The spatial resolved emission(absorption)-line profile may provide information about how feedback change the chemical environment of ICM and CGM and constrain the theoretical models. So Integral field spectroscopy(IFS) is for these studies. Harrison et al. (2014) used integral field unit(IFU) observations covering OIII$\lambda\lambda 4959, 5007$ and Hβ emission lines to study the outflows of 16 type-2 AGN at z<0.2, they found high-velocity ionized gas with observed spatial extents of 6-16kpc. their study demonstrates that galaxy-wide energetic outflows are not confined to the most extreme star-forming galaxies or radio-luminous AGN. Rupke et al. (2019) shows optical integral field observations of the low-redshift galaxy SDSS J211824.06+001729.4 with KCWI, the OII lines at wavelengths of 3726 and 3729 angstroms reveal an ionized outflow spanning 80 by 100 square kiloparsecs.

Comparing with low-redshift observation, observation for high-redshift outflow is insufficient in contrast to how dramatic galaxy evolution at this epoch. Several pieces of observational evidence suggest that the most dramatic galaxy evolution occurred at high redshift($z \approx 1-3$). Firstly, the cosmic space density of BH growth peaks at $z \approx 1-2$ while over half of the integrated BH growth occurred around these redshift(Schmidt & Green (1983);Richards et al. (2006)). Secondly, the peak density of the most intensely star-forming galaxies is at $z \approx 2$(Chapman et al. (2005);Wardlow et al. (2011)), with the peak in cosmic star formation density occurring at the same stage(Madau et al. (1996);Lilly et al. (1999);Madau & Dickinson (2014)). Studies of local galaxies have also suggested that massive galaxies formed the bulk of their stars at high redshift($z \geqslant 1-2$). In conclusion, this is an essential stage for galaxy evolution, outflow observation of this epoch is crucial to reveal how galaxies co-evolve with their environments.

Motivated by the above reasons, in this paper we report a follow-up observation on the famous overdensity field centering on BOSS1441 with Keck Cosmic Web Imager(KCWI). This is an extremely overdense region at $z \approx 2.3$ known as MAMMOTH-1 which was found by Cai et al. (2015). He shows that BOSS1441 has an Lyα emitter(LAE) obverdensity $\delta \approx 10$. Also, the Mayall-4m telescope NB imaging shows that an enormous lyα nebulae with projected size$\geqslant$ 400kpc covers this region(Cai et al. (2017)). All of this shows this is a very interesting field at high redshift. In Section 2 we give details of IFU observations. In Section 3 we present the results and model used to estimate outflow energy and in Section 4 we discuss the lyα nebula and the possible mechanism to power the strong outflow. Finally we give a brief summary in Section 5. Throughout this paper, we assume a flat cosmological model with $\omega_\Lambda = 0.7$,$\omega_m = 0.3$ and $H_0 = 70km/s/Mpc$. In this cosmology, 1"$\approx$ 8.2kpc at z=2.3.

2. Observations

In this section, we provide details on the KCWI instrument configurations, observations,data reduction pipeline, and post-processing after standard reduction pipeline

2.1. *KCWI Instrument Configuration*

Keck Cosmic Web Imager(KCWI) is a general purpose, optical IFS that has been installed on the 10m Keck II telescope. KCWI provides seeing-limited imaging from the wavelength of $3500-5700$, and the spectral resolution can be configured from R=1000 to R=20000. The field of view is $20'' \times 33''$ for large slicer, $16'' \times 20''$ for medium slicer and $8'' \times 20''$ for the small slicer. KCWI is optimal for a survey of gasous nebulae at $z \approx 2$ because: (1) KCWI has a high throughput from $3800-4500$,optimal for probing lyα CIV and HeII lines at $z \approx 2$. (2) KCWI has a high spectral-resolution modes(R>4000) which can resolve the gas kinematics and (3) KCWI has a relatively large field-of-view(FoV) to cover extended lyα nebulae. Futhermore, KCWI nicely complements the characteristics of MUSE which thrives at $\lambda > 5000$. Data was taken with the Keck/KCWI instrument in November 2017. The seeing varied in the range of 0.7-1.1 arcsec.

The KCWI observations of BOSS1441 were carried out on UT 2018 May, seeing varied in the range of 0.7-1.1 arcsec(FWHM of the Gaussian at $\approx$ 4000, measured in thee combined 40 min datacubes). For our program, we configured KCWI with thee BM grating and medium slicer which yields a Field of View(FoV) of 16.8" perpendicular to slicer(24 slicers) and 20" along the slicer. This FoV is sufficient to map the gas around quasar host halo to a radius of $\approx$100kpc at $z \approx 2.3$. This setting can provide a spatial sampling of $\frac{20"}{24slicers} \approx 0.67"$ along the slicer and is seeing-limited perpendicular to the slicer. The spectral resl=olution is R=4000. we observed at central wavelengths ranging from $\lambda = 3900-4100$ to conver the Lyα emission of each quasar in the sample.

The total exposure time for BOSS1441 is 40 minutes which consists of four 10-min individual exposures.

3. Results

3.1. *Radio Emission*

Deep VLA observation(Emonts et al. (2019)) discover CO(1-0) emission which trace the cold molecular gas (T$\approx$10-100 K) on the central source of MAMMOTH-1(we use the terminology in Cai et al. (2017) and call it source-B in following sections) and its companions with the D-configuration of VLA and centered on the frequency of 34.808 GHz(ν_{rest}=115.27 GHz). After 14 hrs exposure, the results shows extended peak radio flux which has 5 kpc offset from the stellar body of source-B (30 kpc beyond 3σ) and 3 faint radio sources in the same region. However, no continuum radio source was found near Source-B. We check

the continuum image of Emonts et al. (2019) and give an upper limit on its submillimeter emission, $f_\nu < 0.01mJy$ at $\lambda_{obs} = 8500\mu m$. But from the results of Arrigoni Battaia et al. (2018)(Fig. 11), this upper limit still cannot rule out the the radio-loud case. But neither the VLA nor ALMA observations detected two distinct radio sources around Source-B, we conclude that Source-B is most likely radio-quiet source.

3.2. *Morphology and Emission*

Fig. **??** shows the HST image of MAMMOTH-1 with WFC F160W filter with contours for Lyα HeII and CIV emission. All sources marked here are at z=2.3 confirmed by CO(1-0) emission(Emonts et al. (2019)) and CO(3-2) emission(Qiong (in prep)). It shows Lyα emission extended $>$ 20" which corresponds to $\approx$ 170kpc, this is the typical size of halo at this redshift. It covers all 8 sources here, this indicates that all of this sources could have contribution to illuminate this nebulae. Size of this nebulae is limited by the FoV of KCWI which is 20" $\times$ 16.8" and is not sensitive enough at the edges. Furthermore, we clearly see that there are three peaks around Source-B, two out of the three peaks are on both sides of the G-5 respectively(Fig.**??**). Besides, HeII and CIV emission also show extent signals(>3σ) which extend to $\approx$ 10" (physical projected scale of 85kpc) in the north-south direction(CIV emission even cover G-5).

Fig. **??** shows spectra extract in 1 $arcsec^2$ aperture centering on the flux peaks. We fit the three emission lines with single component gaussian function and also use the central wavelength fitted to calculate their redshifts, moreover we calculate their luminosity beyond 3σ. We show these results and the fitting parameters in Tab. 1.

	$\lambda_c(A)$	$\sigma_\lambda(A)$	L(erg/s)	redshift
Lyα	4024	7	2.68×10^{44}	2.310
HeII	5438	8	1.97×10^{43}	2.316
CIV	5143	13	2.29×10^{43}	2.320

Table 1:

3.3. *Kinematics*

In this section we present maps of the flux-weighted velocity centroid and the flux-weighted velocity dispersion for the three emission line to get an indication of the centroid velocity and width of the emission line for each spatial location. Different emission line traces different gas component. We use lyα to trace cool gas(10^4K) and use CIV(λ1549),HeII(λ1640) emission to trace warm gas(10^5K). These resolved kinematic maps give us the opportunity to the kinematic structure of this area, evidence for rotation, inflows or outflows and help us to have a deep insight look to the physics of this nebula. We filter the spectra with lowpass filter to reduce the noise, this procedure can help us to construct a more clear velocity and velocity dispersion map, we show the results in Fig. **??**

Left panel is the continuum-subtracted, pseudo-narrowband image, contours represent the SNR levels. Middle panel shows velocity maps and right panel is velocity dispersion map. It is clear that all of the three velocity map show velocity gradient around Source-B and along the same direction, besides, Lyα emission also presents a extended region around Source-B with dispersion larger($\sigma \approx 600km/s$) than other places. With all of these evidence(extent CIV and HeII emission, clear velocity gradient and large velocity dispersion, also the OIII emissionCai et al. (2017)), we think Source-B produces outflow and injects matter and energy into CGM. What is interesting is that the velocity of outflow is still large enough $\approx$ 500km/s in a large distance($\approx$ 100kpc). Because Source-B is radio quiet, this outflow cannot be driven by jet from AGN, AGN-radiation-driven feedback and star-forming-driven feedback are possible. This may be the first observation for the outflow influence on such large scale at high redshift. In addition, it is also clear seen that velocity map shows velocity gradient around G-5, direction of this velocity gradient is parallel to the connection of the two peaks on each side of G-5, dispersion around G-5 also shows a large value comparing with other regions, these evidences may indicate G-5 also produces outflow.

To have a deep insight, we bin the data cube with interval length of 200km/s and show the results in Fig. **??**. It shows significant separate red and blue component on either side of source-B. So does G-5, but the signal is relatively weaker than Source-B instead.

To further explore the physical mechanism here, we extract spectra from different regions of lyα nebula and construct a "spectral map", Fig.**??** shows the result. We construct aperture with radius of $1arcsec^2$ and extract spectra from different part of Lyα neubulae. We also fit lines with one-component gaussian function and show the fitting parameter in Tab. **??**. We clearly see in some regions close to source-B the dispersion is really large even $>$ 600km/s which corresponds to FWHM$>$ 1400km/s. It's hard to imagine anything other than an outflow could cause such a large dispersion.

3.4. *Model of the outflow*

The mass rate, energy rate and momentum rate being carried by outflow are important to help us understand the physical mechanisms to drive it. Although outflow are likely to be entraining gas in multiphases, the cool and warm gas observed here could represent a large fraction of the overall mass and energy of the total outflows. Bscause of the complication of modeling outflows, here we adopt simple outflow models to provide first order constraints. We calculate the upper and lower limit of the outflow energy rate with 2 different ways and the fiducial value we use is their mean in log space(follow the method given by Harrison et al. (2014) The upper limit is given by Rodrguez Zaurn et al. (2013) , we use

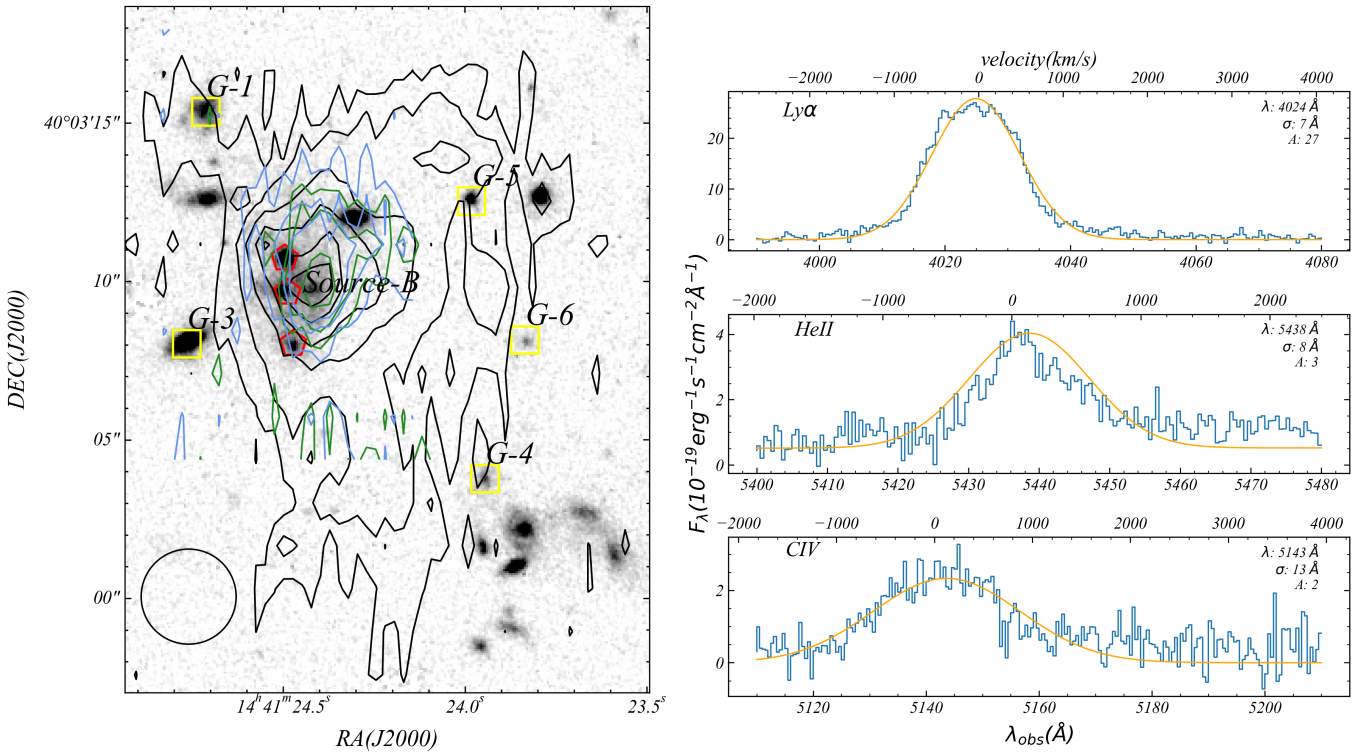

(a) contour (b) spectra

Figure 1: Left: HST image of MAMMOTH-1 from circle 24,25, PI: Cai. We overlay on it Lyα HeII and CIV psudo narrow band images. Black contour is Lyα, blue contour is HeII, green contour is CIV. We also mark source-B with red mark and sources at the same redshift with yellow mark. We also plot circle with raidus of $1arcsec^2$. Right: spectra of the 3 emission lines extracted from aperture center on source-B with radius $1arcsec^2$, we fit them with one-component gaussian function.

Number	1	4	5	7	8	9	10	11	12	13	14	15	16	17	18	19	20	24	25
Velocity(km/s)	-416	-785	-649	-419	-515	-453	208	-157	-257	-424	-211	9	-75	-300	49	236	-267	182	-208
Dispersion(km/s)	618	342	392	626	319	474	450	174	219	444	269	415	799	242	668	481	358	660	472
f_{norm}	0.69	0.63	0.73	0.70	0.79	0.83	0.71	0.84	0.95	0.85	0.91	0.83	0.41	0.86	0.66	0.93	0.81	0.66	0.77

eq. 7 in his paper to calculate the mass outflow rate:

$$\dot{M} = \frac{3Lm_p v_{out}}{\alpha^{eff}_{Ly\alpha} h\nu_{Ly\alpha} n_e r} \quad (1)$$

where L is the luminosity of lymanα emission, m_p is the proton mass, v_{out} is outflow velocity, $alpha_{Ly^{eff}}$ is recombination coefficients, we get this value from Storey & Hummer (1995) , $h\nu_{Ly}$ is the energy of lymanα photons, n_e is electron density, r is the distance we see the outflow from the central AGN, in our case we adopt 30kpc. In addition, the kinetic power of the outflow ($\dot{E}$) is related to the velocity dispersion, mass outflow rate and outflow velocity by:

$$\dot{\mathrm{E}} = \frac{\dot{M}}{2}\left(V^2_{out} + 3\sigma^2\right) \quad (2)$$

the main uncertainty in calculating the mass outflow rates is electron density, this value is often measured from the emission-line ratio SII $\lambda6716/\lambda6731$, this doublet is not covered by our IFU observations, hence, we adopt the value in Cai et al. (2017) $n_e = 1.25cm^{-3}$. With this approch, we obtain $\dot{M}_{out,low} \approx 500\mathrm{M}\odot\ \mathrm{yr}^{-1}$. Moreover with the velocity dispersion we estimated, the energy outflow rate is $\dot{E}_{out,low} \approx 10^{44}erg/s$.

We also consider the mass energy injection rates assuming an energy conserving bubble in a uniform medium Heckman et al. (1990) which gives the relation:

$$\dot{E}_{out,up} \approx 1.5 \times 10^{46} r^2_{10} v^3_{1000} n_{0.5}\ erg/s \quad (3)$$

where r_{10} is the radius in unit of 10kpc, v_{1000} in unit of 1000km/s and $n_{0.5}$ is in unit of $0.5cm^{-3}$. Using this method we obtain values of $E_{out,up} \approx 9 \times 10^{46} erg/s$. The mass outflow rates are then given by $\dot{M}_{out,up} = 2\dot{E}_{out,up}/c^2$ where c is the speed of light, this gives $\dot{M}_{out,up} \approx 8.7 \times 10^5 M_\odot/yr$. So the fiducial value we use is $\dot{E}_{out,mean} = 3 \times 10^{45} erg/s$.

Finally, in preparation for the follow discussion, we estimate outflow momentum rate by taking the mass outflow rate calculated above and assuming $\dot{P}_{out} = \dot{M}_{out} v_{out}$

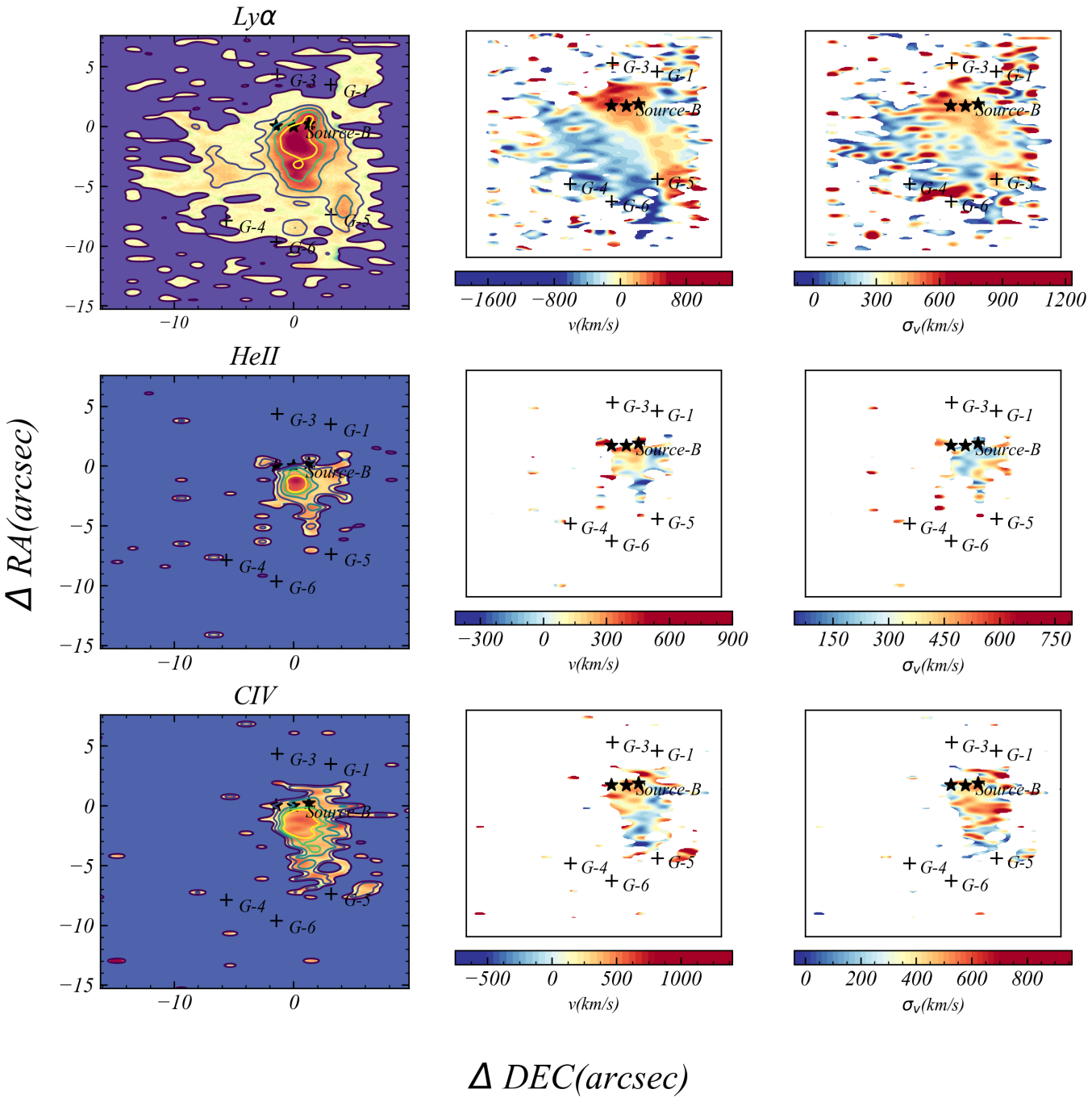

Figure 2: Left: continuum-subtracted psudo-narrow band images for the 3 emissions. We select regions $> 1.5\sigma$ in each slice and stack these slices together. The contour represent signal-to-noise ratio(SNR), for lyα is $(5\sigma, 9\sigma, 18\sigma, 30\sigma, 42\sigma, 51\sigma)$, for HeII is $(3\sigma, 5, 9\sigma)$ and for CIV is $(4\sigma, 7\sigma, 9\sigma)$. Middle: flux-weighted velocity map with respect to the systemic redshift of MAMMOTH-1. Right: flux-weighted velocity dispersion also with respect to systemic redshift of MAMMOTH-1. We also mark sources in the field with cross.

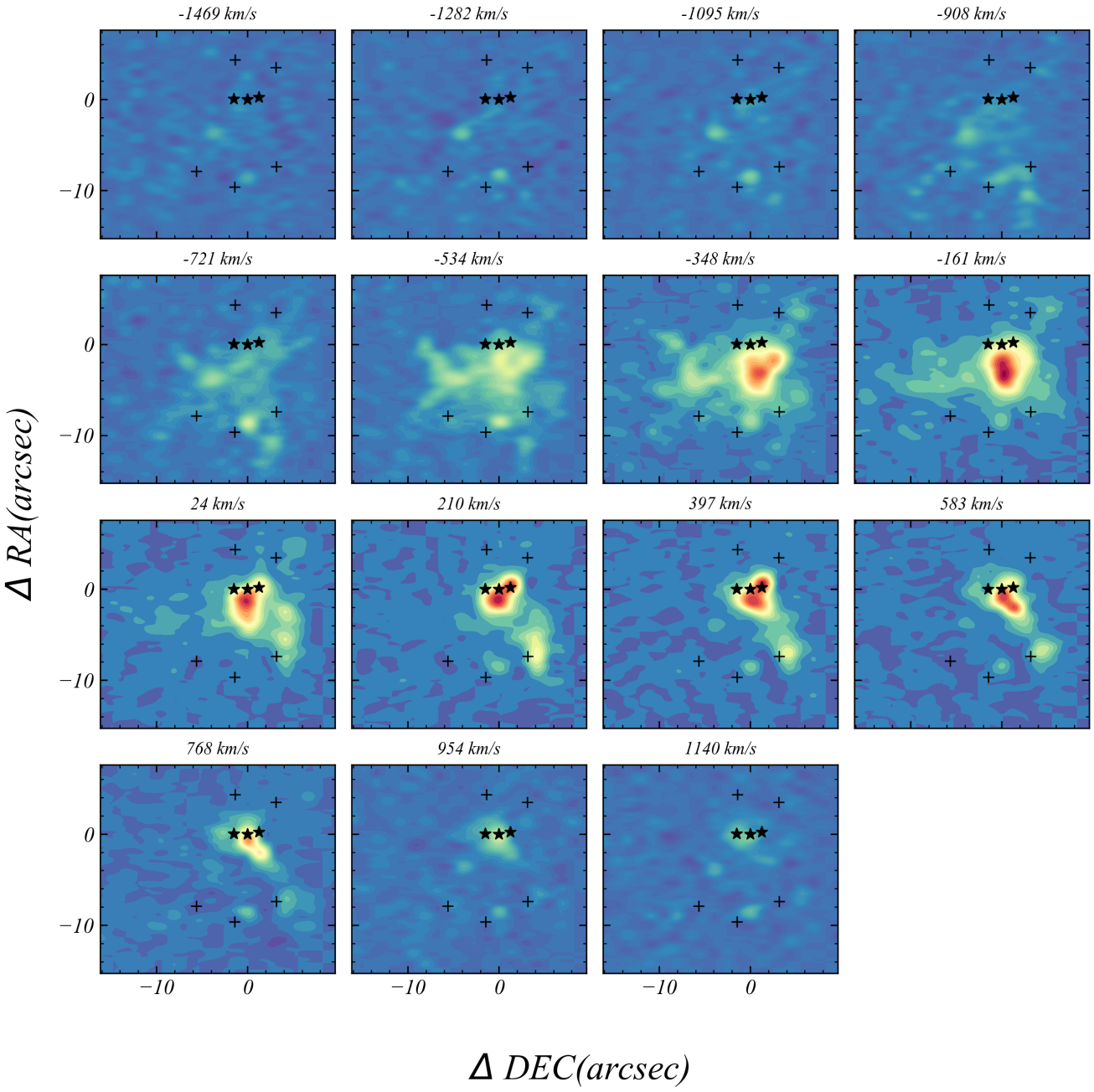

Figure 3: Kinematics of cool gas. It shows signal of lyα emission at different veliocities. We select $\Delta v = 187$km/s which corresponds $4A$ as the bin size of these slices. We extract these slices within the range $4000A - 4040A$, for each image here, we use the mean velocity of the bin as title for each image. It shows significant red and blue component on either side of source-B.

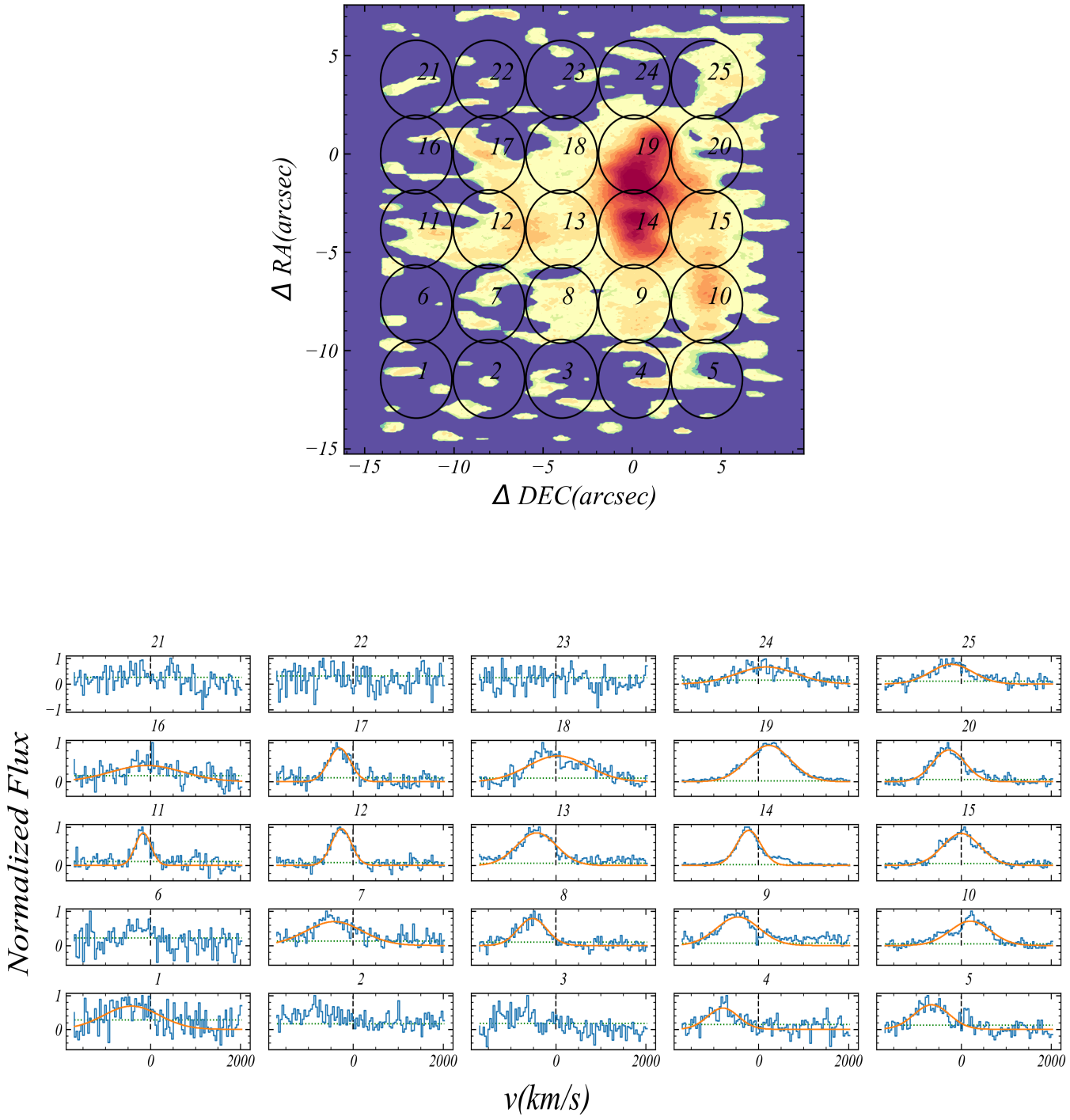

Figure 4: Up: Continuum-subtracted psudo narrow band image of lyα. We overlay circles on it and number them from 1 to 25. Low: Continuum-subtracted spectra extracted from individual spatial regions indicated in upper panel. The apertures are circle with radius of $2arcsec^2$. We number the spectra from 1 to 25 which corresponds to circles in upper panel. We fit the emission line with single gaussian function and show it with orange lines. The green lines show the noise level calculated from the high-frequency component of spectra.

4. Discussion

4.1. *What drives the outflow?*

In this section we will investigate which of these processes could responsible for driving the extreme outflows observed. The dominant processes that drive such large scale outflow in protocluster and the efficiency to which they are able to couple the gas are currently sources of uncertainty in galaxy formation models. Several possible mechanisms have been suggested to drive galaxy-wide outflows, for example: the stellar wind and supernovae; radiation pressure from the extremely luminous AGN or star formation; the interaction of radio jets with a clumpy and multiphase interstellar medium; AGN wind initially launched from the accretion disc. Following Harrison et al. (2014), we calculate the coupling efficiency which is a popular method to investigate the likely drivers of large-scale outflow. We compare the ratio of our outflow kinetic energy rate($\dot{E_{out}}$) with (1) the FIR AGN luminosity; (2) the FIR star formation luminosity (these two power are given by Arrigoni Battaia et al. (2018)). We also calculate the momentum-loading factor for both star-forming-driven case and AGN-driven case. Using these results we now explore the possible driving mechanisms to power this outflow.

Fig.**??** shows coupling efficiency for both star-forming-driven case and AGN-driven case. We compare our result with results in Harrison et al. (2014). One way for star formation to drive large-scale outflow is by stellar winds or supernovae. An estimation of the coupling efficiency for this case is carried by Kennicutt Jr (1998), he found that the maximum coupling efficiency is $\dot{E_{out}}/L_{IR,SF} \approx 0.02$, we indicate this upper limit with gray dot line in Fig.**??**. Based on this results, stellar winds and supernovae are unlikely to be fully responsible for the observed outflows. On the other hand, the coupling efficiency for AGN-driven case is too large which is close to 1. In the right panel of Fig.**??** it shows that if the outflow is driven by AGN, it has already exceed other results with similar AGN luminosity.

Besides, if we instead consider a momentum-driven wind with momentum deposition from the radiation pressure of stars or AGN, the momentum loading factor $f_p = log(c\dot{P_{out}}/L)$ is $f_{p,SF} = 1.7$ and $f_{p,AGN} = 3.2$ respectively. Nevertheless Zubovas (2018) suggests that a typical momentum loading factor for star-formation-driven case is $f_{p,SF} < 1.4$ which is lower than our estimation, this comparison also rules out the star-formation case. In the same way, we also find that $f_{p,AGN}$ is larger than the typical value.

Moreover, Shankar et al. (2006) mentions the two sources of feedback are important over different mass ranges, in particular, stellar feedback regulates the processes in low-mass galaxies while large galaxies are mainly regulated by AGN feedback. The transition mass for this two feedback mechanisms is $M_{tr} \approx 2 \times 10^{10} \mathrm{M}_{\odot}$. By fitting the SED of source-B, Arrigoni Battaia et al. (2018) estimates its stellar mass of source-B to be $\log(M_{\mathrm{star}}/\mathbf{M}_{\odot}) = 11.4^{+0.3}_{-0.2}$. Comparing with M_{tr}, this results also suggests that feedback from star formation is not the dominant reason for the outflow.

However, Zubovas (2018) also suggests there are mechanisms to reach high coupling efficiency and momentum loading factor. One possibility is hyper-Eddington SMBH growth during Compton-thick(heavily obscured) phases. In this case, SMBH would accrete material with extremely large rate and may lead to ultra fast outflows(UFO). Tombesi et al. (2013) shows that this outflow can reach the velocity $\approx 0.1c$ and will have a strong coupling with the interstellar medium(ISM). Fig.6 of Tombesi et al. (2013) shows some coupling efficiency of some UFOs $\approx$ 1, but he also explains that this extremely fast and powerful outflow would occur only very close to SMBH $R \approx 1000 r_s$(where r_s is the schwarzschild radius.). He indicates that the large coupling efficiency is probably due to large environment column density $\approx 10_{24} cm^{-2}$ and highly ionized state. These two factors are consistent with the large-scale environmental conditions(MAMMOTH-1, extreme onverdensities; enomous lymanα nebula.). Nevertheless, Cai et al. (2017) suggests that the hydrogen column density is in the range $\approx 10^{20} cm^{-2}$, we indicate here that the column density in CGM maybe $10^3 cm^{-2}$ larger than this value.

In summary, based on our analyses we find the outflow is unlikely powered by star-forming processes, but we do see some similar behaviors between the outflow and UFO(high coupling efficiency and high momentum loading factor), so we conclude that this outflow maybe driven by accretion-disc winds. Although there's large uncertainty coupling efficiency estimation, this large coupling efficiency and momentum loading factor have never been seen on such a large scale. From the observation it's still unclear what kind of mechanism leads to such large coupling efficiency on such large scale(the typical coupling efficiency beyond 10kpc <0.01), it maybe results from large column density $> 10^{24} cm^{-2}$ or very efficient cooling mechanism. Besides, it provides evidence that outflow from central quasar can truely have influence on the protocluster.

4.2. *Galaxies merger*

By the submillimeter observation with ALMA and data collection from literature, Arrigoni Battaia et al. (2018) fits the spectral energy distribution(SED) for Source-B, as a results he indicates that Source-B is an Ultra-Luminous Infrared Galaxy(ULIRG) with extreme far-infared luminosity. Besides, Treister et al. (2010) shows that there is substantial observational evidence that ULIRGs(heavily obscured galaxies) are the product of the gas-rich merger of two massive galaxies. Cai et al. (2017) also shows Source-B is a strongly obscured source. On the other hand the the flux-weighted dispersion map of lyα emission also shows velocity dispersion $> 600 km/s$ corresponding to FWHM $> 1400 km/s$ near Source-B and the large dispersion extent to projected scale $\approx 100 kpc$(include G-5). Moreover, MAMMOTH-1 is an extreme overdensity($\delta = 10.8 \pm 2.6$), The three sources of source-B is within 70 kpc. All of these evidences suggests a strong galaxies merger in this region.

We suggest that the physical picture of this area is like this: three sources of source-B is experiencing galaxy merger, cen-

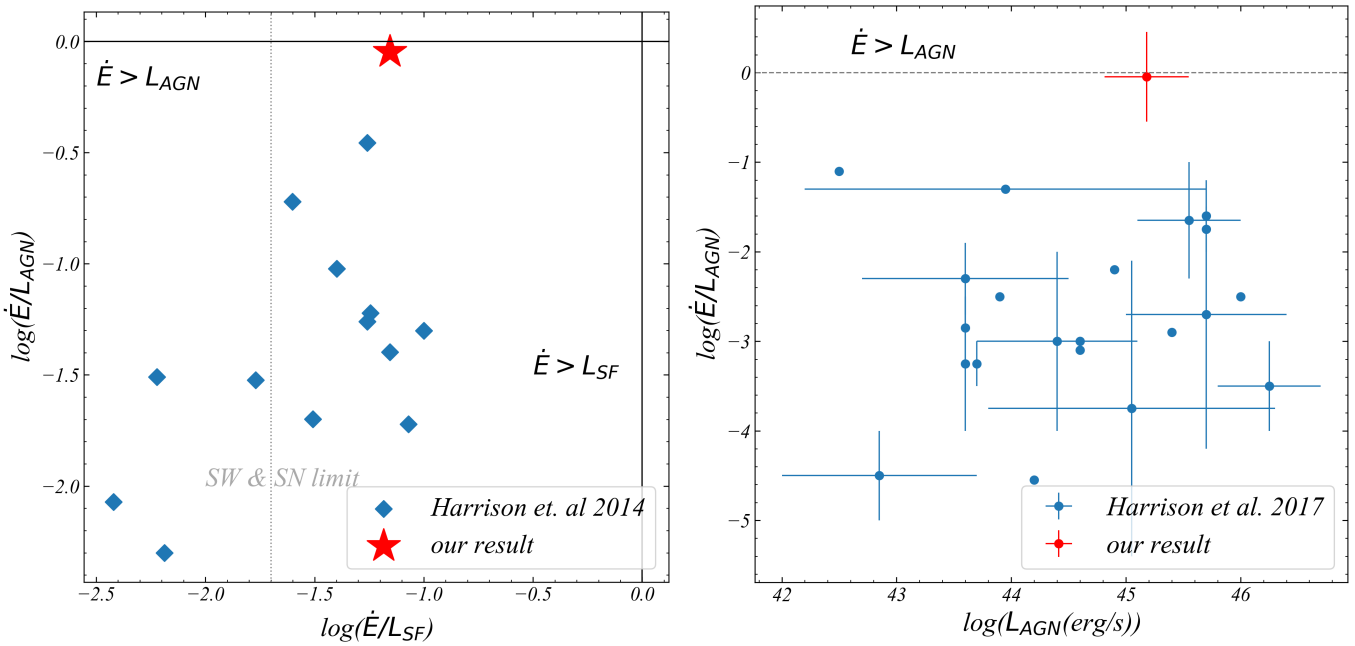

Figure 5: Left: the ratio of our estimated outflow kinetic energy rates(E_{out}) to the AGN luminosity and to the star formation luminosity for our source(red) and sources from Harrison et al. (2014). The dashed vertical line is the estimated maximum mechanical input expected from supernovae and stellar winds. The two solid lines shows the coupling efficiency of 1. Right: Observationally determined kinetic coupling efficiencies in Harrison et al. (2018) and our result. The vertical lines show the range of values quoted or, in the case of an error bar, the quoted error on the average value. The horizontal lines show the range of bolometric luminosity for each sample. The dotted line shows coupling efficiency of 1.

ter source accretes gas and material the other two sources, its super massive black hole(SMBH) is going through a period of rapid growth and produce strong outflow. Owing to the tidal effect between the three sources, lots of material is pulled out from galaxies to CGM. This can also explain why there's such large coupling efficiency between outflow and environment.

Futhermore, from the velocity and dispersion map we see that the region with large dispersion extent to G-5 and there's also obvious velocity gradient on either side of G-5. This clue indicates that there may be also outflow from G-5. The large dispersion also support this point.

5. Conclusions

References

Arrigoni Battaia, F., Hennawi, J. F., Prochaska, J. X., Oñorbe, J., Farina, E. P., Cantalupo, S., & Lusso, E. 2018, Monthly Notices of the Royal Astronomical Society, 482, 3162

Benson, A., Bower, R., Frenk, C., Lacey, C. G., Baugh, C., & Cole, S. 2003, The Astrophysical Journal, 599, 38

Borgani, S., Fabjan, D., Tornatore, L., Schindler, S., Dolag, K., & Diaferio, A. 2008, Space Science Reviews, 134, 379

Bower, R. G., Benson, A., Malbon, R., Helly, J., Frenk, C., Baugh, C., Cole, S., & Lacey, C. G. 2006, Monthly Notices of the Royal Astronomical Society, 370, 645

Cai, Z. et al. 2015, arXiv preprint arXiv:1512.06859

Cai, Z. et al. 2017, The Astrophysical Journal, 837, 71

Chapman, S. C., Blain, A., Smail, I., & Ivison, R. 2005, The Astrophysical Journal, 622, 772

Churazov, E., Sazonov, S., Sunyaev, R., Forman, W., Jones, C., & Böhringer, H. 2005, Monthly Notices of the Royal Astronomical Society: Letters, 363, L91

Ciotti, L., Ostriker, J. P., & Proga, D. 2010, The Astrophysical Journal, 717, 708

Croton, D. J. et al. 2006, Monthly Notices of the Royal Astronomical Society, 365, 11

DeBuhr, J., Quataert, E., & Ma, C.-P. 2012, Monthly Notices of the Royal Astronomical Society, 420, 2221

Emonts, B. H., Cai, Z., Prochaska, J. X., Li, Q., & Lehnert, M. D. 2019, The Astrophysical Journal, 887, 86

Fabian, A. 1999, Monthly Notices of the Royal Astronomical Society, 308, L39

Fabjan, D., Borgani, S., Tornatore, L., Saro, A., Murante, G., & Dolag, K. 2010, Monthly Notices of the Royal Astronomical Society, 401, 1670

Faucher-Giguère, C.-A., & Quataert, E. 2012, Monthly Notices of the Royal Astronomical Society, 425, 605

Granato, G. L., De Zotti, G., Silva, L., Bressan, A., & Danese, L. 2004, The Astrophysical Journal, 600, 580

Harrison, C., Alexander, D., Mullaney, J., & Swinbank, A. 2014, Monthly Notices of the Royal Astronomical Society, 441, 3306

Harrison, C., Costa, T., Tadhunter, C., Flütsch, A., Kakkad, D., Perna, M., & Vietri, G. 2018, Nature Astronomy, 2, 198

Harrison, C. M. 2016, Observational constraints on the influence of active galactic nuclei on the evolution of galaxies (Springer)

Heckman, T. M., Armus, L., Miley, G. K., et al. 1990, Astrophysical Journal Supplement Series, 74, 833

Hopkins, A. M., & Beacom, J. F. 2006, The Astrophysical Journal, 651, 142

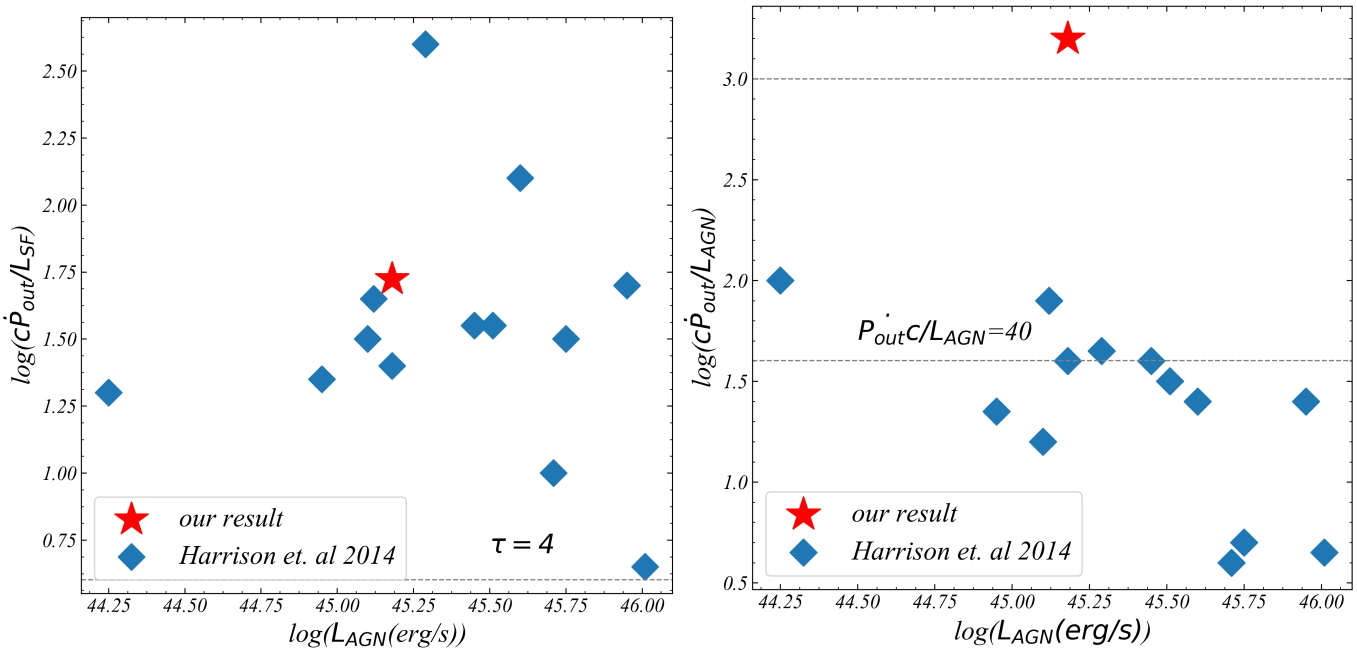

Figure 6: Left: momentum rates of the outflows($\dot{P_{out}}$ normalized to the star formation luminosity L_{SF}/c versus AGN luminosity. The dashed lines represent the required optical depths if the outflows are driven by radiation pressure from star formation. Right: momentum rate of outflows normalized to AGN luminosity(L_{AGN}/c) versus AGN luminosity. Based on our assumptions, the outflows are unlikely to be purely radiatively driven, the ratio is also to high for theoretical predictions of energy-driven outflows launched by AGN accretion-disc wind.

Ishibashi, W., & Fabian, A. 2012, Monthly Notices of the Royal Astronomical Society, 427, 2998

Kennicutt Jr, R. C. 1998, Annual Review of Astronomy and Astrophysics, 36, 189

King, A., Zubovas, K., & Power, C. 2011, Monthly Notices of the Royal Astronomical Society: Letters, 415, L6

Lilly, S. J., Eales, S. A., Gear, W. K., Hammer, F., Le Fèvre, O., Crampton, D., Bond, J. R., & Dunne, L. 1999, The Astrophysical Journal, 518, 641

Madau, P., & Dickinson, M. 2014, Annual Review of Astronomy and Astrophysics, 52, 415

Madau, P., Ferguson, H. C., Dickinson, M. E., Giavalisco, M., Steidel, C. C., & Fruchter, A. 1996, Monthly Notices of the Royal Astronomical Society, 283, 1388

McCarthy, I. G., Schaye, J., Bower, R. G., Ponman, T. J., Booth, C. M., Vecchia, C. D., & Springel, V. 2011, Monthly Notices of the Royal Astronomical Society, 412, 1965

Mullaney, J., Alexander, D., Fine, S., Goulding, A., Harrison, C., & Hickox, R. 2013, Monthly Notices of the Royal Astronomical Society, 433, 622

Nayakshin, S., & Zubovas, K. 2012, Monthly Notices of the Royal Astronomical Society, 427, 372

Nesvadba, N., Lehnert, M., De Breuck, C., Gilbert, A., & Van Breugel, W. 2008, Astronomy & Astrophysics, 491, 407

Richards, G. T. et al. 2006, The Astronomical Journal, 131, 2766

Rodrguez Zaurn, J., Tadhunter, C., Rose, M., & Holt, J. 2013, Monthly Notices of the Royal Astronomical Society, 432, 138

Rupke, D. S. et al. 2019, Nature, 574, 643

Schmidt, M., & Green, R. 1983, The Astrophysical Journal, 269, 352

Shankar, F., Lapi, A., Salucci, P., De Zotti, G., & Danese, L. 2006, The Astrophysical Journal, 643, 14

Silk, J. 2013, The Astrophysical Journal, 772, 112

Somerville, R. S., Hopkins, P. F., Cox, T. J., Robertson, B. E., & Hernquist, L. 2008, Monthly Notices of the Royal Astronomical Society, 391, 481

Storey, P., & Hummer, D. 1995, Monthly Notices of the Royal Astronomical Society, 272, 41

Tombesi, F., Cappi, M., Reeves, J., Nemmen, R., Braito, V., Gaspari, M., & Reynolds, C. 2013, Monthly Notices of the Royal Astronomical Society, 430, 1102

Treister, E., Natarajan, P., Sanders, D. B., Urry, C. M., Schawinski, K., & Kartaltepe, J. 2010, Science, 328, 600

Wang, K., Zhang, Q., Wu, Y., & Zhang, H. 2011, The Astrophysical Journal, 735, 64

Wardlow, J. L. et al. 2011, Monthly Notices of the Royal Astronomical Society, 415, 1479

Wiersma, R. P., Schaye, J., Theuns, T., Dalla Vecchia, C., & Tornatore, L. 2009, Monthly Notices of the Royal Astronomical Society, 399, 574

Zubovas, K. 2018, Monthly Notices of the Royal Astronomical Society, 479, 3189